Accepted Manuscript

A comparison of macroscopic models describing the collective response of sedimenting rod-like particles in shear flows

Christiane Helzel, Athanasios E. Tzavaras

PII: S0167-2789(15)30183-4
DOI: http://dx.doi.org/10.1016/j.physd.2016.07.004
Reference: PHYSD 31832

To appear in: *Physica D*

Received date: 12 October 2015
Revised date: 13 June 2016
Accepted date: 11 July 2016

Please cite this article as: C. Helzel, A.E. Tzavaras, A comparison of macroscopic models describing the collective response of sedimenting rod-like particles in shear flows, *Physica D* (2016), http://dx.doi.org/10.1016/j.physd.2016.07.004

A comparison of macroscopic models describing the collective response of sedimenting rod-like particles in shear flows.

Christiane Helzel* Athanasios E. Tzavaras †

Abstract

We consider a kinetic model, which describes the sedimentation of rod-like particles in dilute suspensions under the influence of gravity, presented in [8]. Here we restrict our considerations to shear flow and consider a simplified situation, where the particle orientation is restricted to the plane spanned by the direction of shear and the direction of gravity. For this simplified kinetic model we carry out a linear stability analysis and we derive two different nonlinear macroscopic models which describe the formation of clusters of higher particle density. One of these macroscopic models is based on a diffusive scaling, the other one is based on a so-called quasi-dynamic approximation. Numerical computations, which compare the predictions of the macroscopic models with the kinetic model, complete our presentation.

Key words: rod-like particles, sedimentation, linear stability, moment closure, quasi-dynamic approximation, diffusive scaling

1 Introduction

We discuss different mathematical models which describe the sedimentation process for dilute suspensions of rod-like particles under the influence of gravity. The sedimentation of rod-like particles has been studied by several authors in theoretical as well as experimental and numerical works, see Guazzelli and Hinch [5] for a recent review paper. Experimental studies of Guazzelli and coworkers [9, 10, 12] start with a well stirred suspension. Under the influence of gravity, a well stirred initial configuration is unstable and it is observed that clusters with higher particles concentration form. These clusters have a mesoscopic equilibrium width. Within a cluster, individual particles tend to align in the direction of gravity.

The basic mechanism of instability and cluster formation was described in a fundamental paper of Koch and Shaqfeh [11]. In Helzel and Tzavaras [8], we recently derived a kinetic model which describes the sedimentation process for dilute suspensions of rod-like particles. By applying moment closure hypotheses and other approximations to an associated moment system, we derived macroscopic models for the evolution of the rod density and compared the prediction of such macroscopic models to the original kinetic model using numerical experiments. This is done in [8] for rectilinear flows with the particles taking values on the sphere.

*Institute of Mathematics, Heinrich-Heine-University Düsseldorf, Düsseldorf, Germany. christiane.helzel@hhu.de

†Computer, Electrical, Mathematical Sciences & Engineering Division, King Abdullah University of Science and Technology (KAUST), Thuwal, Saudi Arabia. athanasios.tzavaras@kaust.edu.sa

In the present work, in order to explain our approach, we restrict our analysis to the simpler case of shear flows for particles with orientations restricted to take values on the plane. While the derivations in [8] are often quite technical, the restriction to this simpler situation provides a useful and technically simple setting in order to understand the underlying ideas. In addition, it turns out that the form of the derived macroscopic equations is identical in both cases apart from the values of numerical constants that capture the effect of dimensionality in the microstructure. Therefore, we hope that this paper will make our results accessible and useful to a wider community interested in the modelling of complex fluids. Moreover, we also consider an alternative route to closure at the density level via diffusive scaling. The closure via diffusive scaling leads to the classical Keller-Segel system while the quasi-dynamic approximation leads to a variant of a flux-limited Keller-Segel system. The different effective equations are numerically compared among each other and also compared with a computation of the full nonlinear kinetic model.

The article is organised as follows: In Section 2, we present the kinetic model from [8] and the non-dimensionalization of the problem. For vertical shear flows we derive a simplified one-space dimensional model, obtained by restricting the orientation of particles to move in a plane. In Section 3 a nonlinear moment closure system is derived (see (38)-(41)) which forms the basis for all further considerations. Effective equations for the evolution of the macroscopic density are obtained via two approaches: Starting from the moment system (38)-(41) in Section 4, we employ a quasi-dynamic approximation and derive an effective equation for the evolution of the macroscopic density. The approximation amounts to replacing the dynamical behavior of the second order moments by enslaving the second-order moments to their respective local equilibria. An alternative approach is presented in Section 5 and Appendix A, where the effective equation for the density is obtained directly from the kinetic equation via a diffusive limit. The diffusive approximation leads to the well known Keller-Segel model (52), while the quasi-dynamic approximation leads to a flux-limited Keller-Segel type model (46).

In Section 6 we present numerical results comparing the diffusive approximation and the quasi-dynamic approximation to the full kinetic model. Although the idea of diffusive scalings to obtain macroscopic equations is commonplace in kinetic theory (see [3, 13, 6]), it has not been applied (to our knowledge) in the sedimentation problem. The derivation of the hyperbolic and diffusive scaling equations for general rectilinear flows is presented in Appendix A for the general case where the directions of the rod-like particles take values on the sphere. Finally, in Appendix B, we present a stability analysis for the linearized moment closure system to establish the linear instability of the rest state under a shear flow perturbation. It turns out that a nonzero Reynolds number provides a wavelength selection mechanism. An asymptotic analysis of the largest eigenvalue around $Re = 0$ explains this behavior.

2 A kinetic model for the sedimentation of rod-like particles

We describe a kinetic model for sedimentation in dilute suspensions of rod-like Brownian particles, following Doi and Edwards [4, Ch. 8]; see also [14] and [7]. The model accounts for the effects of gravity and hydrostatic interactions in a dilute suspension (see [8]).

Consider a suspension consisting of inflexible rod-like particles of thickness b and length l, with $b \ll l$, submerged in a solvent extending over the entire space. The rods are subjected to a gravity field $\boldsymbol{g} = -g\boldsymbol{e}_3$, with gravitational constant g and where $\boldsymbol{e}_3$ is the unit vector in the upward direction. If m_0 denotes the mass of an individual particle then $\boldsymbol{G} = -m_0 g\boldsymbol{e}_3$ is the force of gravity on a single particle. Some of our basic notation is depicted in Figure 1.

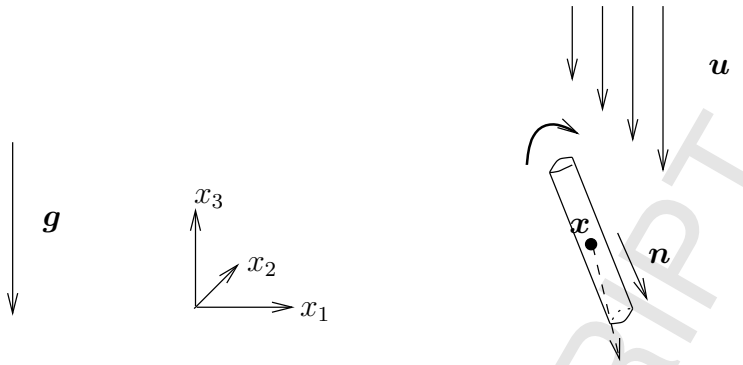

Figure 1: Basic notation for rod-like molecule which is falling sidewards.

The motion of the particles is friction dominated. If $\boldsymbol{u}(\boldsymbol{x},t)$ stands for the velocity field of the solvent, then a rigid particle is described by the position $\boldsymbol{x}\in\mathbb{R}^d$ of the center of mass and the orientation $\boldsymbol{n}\in S^{d-1}$ of the rod. Kinematic considerations dictate that each rod obeys the equations

$$\begin{aligned}\frac{d\boldsymbol{x}}{dt}&=\boldsymbol{u}+\left(\frac{1}{\zeta_{||}}\boldsymbol{n}\otimes\boldsymbol{n}+\frac{1}{\zeta_{\perp}}\left(I-\boldsymbol{n}\otimes\boldsymbol{n}\right)\right)\boldsymbol{G}\\ \frac{d\boldsymbol{n}}{dt}&=P_{\boldsymbol{n}^{\perp}}\nabla_{\boldsymbol{x}}\boldsymbol{u}\boldsymbol{n}\end{aligned}$$

where

$$P_{\boldsymbol{n}^{\perp}}\nabla_{\boldsymbol{x}}\boldsymbol{u}\boldsymbol{n}=\big(I-\boldsymbol{n}\otimes\boldsymbol{n}\big)(\nabla_{\boldsymbol{x}}\boldsymbol{u})\boldsymbol{n}$$

is the projection of the vector $(\nabla_{\boldsymbol{x}}\boldsymbol{u})\boldsymbol{n}$ onto the tangent space at $\boldsymbol{n}$, while $\zeta_{||}$ and $\zeta_{\perp}$ are the frictional coefficients in the tangential and the normal direction. Note that $\zeta_{\perp}=2\zeta_{||}$, see [4, App 8.I], implying that a particle with a vertical orientation sediments twice as fast as a particle with horizontal orientation while a particle of oblique orientation moves also sideways.

Upon including the effects of rotational and translational Brownian motion the kinematics of the microstructure is described by the system of stochastic differential equations

$$\begin{aligned}d\boldsymbol{x}&=\Big[\boldsymbol{u}+\Big(\frac{1}{\zeta_{||}}\boldsymbol{n}\otimes\boldsymbol{n}+\frac{1}{\zeta_{\perp}}\left(I-\boldsymbol{n}\otimes\boldsymbol{n}\right)\Big)\boldsymbol{G}\Big]\,dt+\sqrt{\frac{2k_B\theta}{\zeta_{||}}\boldsymbol{n}\otimes\boldsymbol{n}+\frac{2k_B\theta}{\zeta_{\perp}}(I-\boldsymbol{n}\otimes\boldsymbol{n})}\,dW\\ d\boldsymbol{n}&=P_{\boldsymbol{n}^{\perp}}\nabla_{\boldsymbol{x}}\boldsymbol{u}\boldsymbol{n}\,dt+\sqrt{\frac{2k_B\theta}{\zeta_r}}\,dB\end{aligned}\tag{1}$$

where W is the translational Brownian motion and B the rotational Brownian motion, ζ_r the rotational friction coefficient, k_B the Boltzmann constant and θ the absolute temperature.

We consider a suspension of many such molecules in the dilute regime, characterized by the relation $\nu l^3\ll 1$. In this regime the average distance of molecules is much larger than their length and the molecules remain nearly statistically independent. By the law of large numbers the empirical distribution of particles as a function of the center of mass $\boldsymbol{x}$ and orientation $\boldsymbol{n}$ is well approximated by a probability distribution $f(t,\boldsymbol{x},\boldsymbol{n})\,d\boldsymbol{n}d\boldsymbol{x}$. By the equivalence of drift-diffusion equations and Fokker-Planck equations, the dynamics can be described by the

Smoluchowski equation

$$\begin{aligned}\partial_t f + \nabla_{\boldsymbol{x}} \cdot \left[\left(\boldsymbol{u} + \frac{1}{\zeta_\perp}\left(\boldsymbol{n}\otimes\boldsymbol{n} + I\right)\boldsymbol{G}\right) f\right] + \nabla_{\boldsymbol{n}} \cdot \left(P_{\boldsymbol{n}^\perp} \nabla_{\boldsymbol{x}} \boldsymbol{u}\boldsymbol{n} f\right) \\ = \frac{k_B\theta}{\zeta_r}\Delta_{\boldsymbol{n}} f + \frac{k_B\theta}{\zeta_\perp}\nabla_{\boldsymbol{x}} \cdot \left(\boldsymbol{n}\otimes\boldsymbol{n} + I\right)\nabla_{\boldsymbol{x}} f.\end{aligned} \tag{2}$$

Here, $\nabla_{\boldsymbol{x}}$ and $\nabla_{\boldsymbol{x}}\cdot$ denote the usual gradient and divergence in the macroscopic flow domain. On the other hand, $\nabla_{\boldsymbol{n}}$ stands for the surface gradient operator (on the sphere), acting on a scalar function $\varphi = \varphi(\boldsymbol{n})$ by the formula $\nabla_{\boldsymbol{n}}\varphi = \nabla\varphi - \boldsymbol{n}(\boldsymbol{n}\cdot\nabla\varphi)$ where ∇ stands for the usual gradient operator. The gradient, divergence and Laplacian on the sphere are denoted by $\nabla_{\boldsymbol{n}}$, $\nabla_{\boldsymbol{n}}\cdot$ and $\Delta_{\boldsymbol{n}}$, The second term on the left hand side of (2) models transport of the center of mass of the particles due to the macroscopic flow velocity and due to gravity. The last term on the left hand side models the rotation of the axis due to a macroscopic velocity gradient $\nabla_{\boldsymbol{x}}\boldsymbol{u}$. The terms on the right hand side describe rotational as well as translational diffusion. The translational diffusion is non-isotropic as is also the spatial transport term.

If an initial isotropic distribution of particles is distorted by a velocity gradient $\nabla_{\boldsymbol{x}}\boldsymbol{u}$, this will lead to an increase in entropy. A requirement of thermodynamic consistency (see [4, Sec 8.6]) suggests to define the elastic stress tensor $\sigma(\boldsymbol{x},t)$ induced by the microstructure by

$$\sigma(\boldsymbol{x},t) := k_B\theta \int_{S^{d-1}} \left(d\boldsymbol{n}\otimes\boldsymbol{n} - I\right) f(\boldsymbol{x},t,\boldsymbol{n}) d\boldsymbol{n}. \tag{3}$$

This stress resulting from the suspension is added to the stresses of the solvent (usually assumed to be Newtonian fluid) and produce the total stress.

To derive the equation of motion for the solvent we take into account that local variations in the density $m_0\int_{S^{d-1}} f d\boldsymbol{n}$ of the suspended microstructure lead to spatial variations of the specific weight of the suspension that generally can not be compensated by a hydrostatic pressure and thus trigger a fluid motion (buoyancy). The macroscopic flow is described by the Navier-Stokes equation. If the solvent is an incompressible fluid and its density ρ_f is taken constant, then the balance laws of mass and momentum take the form

$$\begin{aligned}\rho_f\Big(\partial_t\boldsymbol{u} + \left(\boldsymbol{u}\cdot\nabla_{\boldsymbol{x}}\right)\boldsymbol{u}\Big) = \mu\triangle_{\boldsymbol{x}}\boldsymbol{u} - \nabla_{\boldsymbol{x}} p + \nabla_{\boldsymbol{x}}\cdot\sigma - \Big(\int_{S^{d-1}} f d\boldsymbol{n}\Big) m_0 g\boldsymbol{e}_3 \\ \nabla_{\boldsymbol{x}}\cdot\boldsymbol{u} = 0\end{aligned} \tag{4}$$

In (4) we have incorporated in the pressure p, $p = p' + \rho_f g\boldsymbol{e}_3\cdot\boldsymbol{x}$, the hydrostatic pressure caused by the effect of gravity $\rho_f g\boldsymbol{e}_3$ on the solvent.

The equations are collected into a nonlinear system consisting of a kinetic equation coupled to the macroscopic Navier-Stokes system through the zero and second moments of the distribution function :

$$\begin{aligned}\partial_t f = -\nabla_{\boldsymbol{x}}\cdot\left(\boldsymbol{u}f\right) - \nabla_{\boldsymbol{n}}\cdot\left(P_{\boldsymbol{n}^\perp}\nabla_{\boldsymbol{x}}\boldsymbol{u}\boldsymbol{n}f\right) + D_r\Delta_{\boldsymbol{n}} f \\ + D_\perp\nabla_{\boldsymbol{x}}\cdot\left(I + \boldsymbol{n}\otimes\boldsymbol{n}\right)\Big(\nabla_{\boldsymbol{x}} f + \frac{1}{k_B\theta} f\,\nabla_{\boldsymbol{x}} U\Big),\end{aligned} \tag{5}$$

$$\sigma(\boldsymbol{x},t) = k_B\theta\int_{S^{d-1}}\left(d\boldsymbol{n}\otimes\boldsymbol{n} - I\right) f(\boldsymbol{x},t,\boldsymbol{n}) d\boldsymbol{n} \tag{6}$$

$$\nabla_{\boldsymbol{x}}\cdot\boldsymbol{u} = 0 \tag{7}$$

$$\rho_f\left(\partial_t\boldsymbol{u} + \left(\boldsymbol{u}\cdot\nabla_{\boldsymbol{x}}\right)\boldsymbol{u}\right) = \mu\Delta_{\boldsymbol{x}}\boldsymbol{u} - \nabla_{\boldsymbol{x}} p + \nabla_{\boldsymbol{x}}\cdot\sigma - \Big(\int_{S^{d-1}} f\,d\boldsymbol{n}\Big) m_0 g\boldsymbol{e}_3 \tag{8}$$

Here $D_r := \frac{k_B\theta}{\zeta_r}$, $D_\perp := \frac{k_B\theta}{\zeta_\perp}$, and $D_{||} := \frac{k_B\theta}{\zeta_{||}} = 2D_\perp$ stand for the rotational and translational diffusion coefficients and $U(x) = m_0 g(\boldsymbol{x}\cdot\boldsymbol{e}_3)$ is the potential of the gravity force $\boldsymbol{G} = -\nabla U$. The total number of rod-like particles is

$$\int_\Omega \int_{S^{d-1}} f(\boldsymbol{x},t,\boldsymbol{n})\,d\boldsymbol{n}\,d\boldsymbol{x} = \int_\Omega \int_{S^{d-1}} f(\boldsymbol{x},0,\boldsymbol{n})\,d\boldsymbol{n}\,d\boldsymbol{x} = N,$$

i.e. f has dimensions of number density.

Thermodynamical structure of the model. The free energy functional (internal energy minus temperature times entropy) reads

$$A[f] := \int_\Omega \int_{S^{d-1}} (k_B\theta f \ln f + fU(\boldsymbol{x}))\,d\boldsymbol{n}d\boldsymbol{x}, \tag{9}$$

where $U(\boldsymbol{x}) = m_0 g\boldsymbol{x}\cdot\boldsymbol{e}_3$ is the gravitational potential.

We next compute using (9) and (5)

$$\begin{aligned}\partial_t A[f] &= \int_\Omega \int_{S^{d-1}} \Big(k_B\theta(1+\ln f) + U(\boldsymbol{x})\Big) f_t\,d\boldsymbol{n}d\boldsymbol{x} \\ &= I_{tr} + I_{dr} + I_{rd} + I_{td}\end{aligned} \tag{10}$$

where I_{tr}, I_{dr}, I_{rd} and I_{td} stand for the contributions of the transport, rotational drift, rotational diffusion and translational diffusion, respectively, that are computed below.

The computations are based on vector calculus formulas for the surface gradient operator $\nabla_{\boldsymbol{n}}$ that are listed below. Let $\boldsymbol{F} = \boldsymbol{F}(\boldsymbol{n})$ be a vector-valued function and $f = f(\boldsymbol{n})$, $g = g(\boldsymbol{n})$ be scalar-valued functions with $\boldsymbol{n}\in S^{d-1}$, the unit sphere in the d-dimensional space, then

$$\int_{S^{d-1}} (\nabla_{\boldsymbol{n}}\cdot\boldsymbol{F}) f\,d\boldsymbol{n} = -\int_{S^{d-1}} \boldsymbol{F}\cdot(\nabla_{\boldsymbol{n}} f - (d-1)\boldsymbol{n}f)d\boldsymbol{n} \tag{11}$$

$$\int_{S^{d-1}} (\nabla_{\boldsymbol{n}}\cdot\nabla_{\boldsymbol{n}} f) g\,d\boldsymbol{n} = \int_{S^{d-1}} (\nabla_{\boldsymbol{n}}\cdot\nabla_{\boldsymbol{n}} g) f\,d\boldsymbol{n} \tag{12}$$

$$\int_{S^{d-1}} \boldsymbol{n}\otimes\nabla_{\boldsymbol{n}} f\,d\boldsymbol{n} = \int_{S^{d-1}} \nabla_{\boldsymbol{n}} f\otimes\boldsymbol{n}\,d\boldsymbol{n} = \int_{S^{d-1}} (d\boldsymbol{n}\otimes\boldsymbol{n} - \mathrm{I}) f\,d\boldsymbol{n} \tag{13}$$

The contribution of the transport term $-\nabla_{\boldsymbol{x}}\cdot(\boldsymbol{u}f)$ is

$$\begin{aligned} I_{tr} &= -\int_\Omega \int_{S^2} \Big(k_B\theta(1+\ln f) + U(\boldsymbol{x})\Big)\nabla_{\boldsymbol{x}}\cdot(\boldsymbol{u}f)\,d\boldsymbol{n}d\boldsymbol{x} \\ &\overset{(7)}{=} \int_\Omega m_0 g\boldsymbol{e}_3 \left(\int_{S^{d-1}} f d\boldsymbol{n}\right)\cdot\boldsymbol{u}\,d\boldsymbol{x}\end{aligned}$$

The contribution of the drift term $-\nabla_{\boldsymbol{n}}\cdot(P_{\boldsymbol{n}^\perp}\nabla_{\boldsymbol{x}}\boldsymbol{u}\boldsymbol{n}f)$ is :

$$\begin{aligned} I_{dr} &= -\int_\Omega \int_{S^{d-1}} \Big(k_B\theta(1+\ln f) + U(\boldsymbol{x})\Big)\nabla_{\boldsymbol{n}}\cdot(P_{\boldsymbol{n}^\perp}\nabla_{\boldsymbol{x}}\boldsymbol{u}\boldsymbol{n}f)\,d\boldsymbol{n}d\boldsymbol{x} \\ &\overset{(11)}{=} \int_\Omega \int_{S^{d-1}} k_B\theta\nabla_{\boldsymbol{n}}\ln f\cdot P_{\boldsymbol{n}^\perp}(\nabla_{\boldsymbol{x}}\boldsymbol{u}\boldsymbol{n}f)\,d\boldsymbol{n}d\boldsymbol{x} \\ &= \int_\Omega \nabla_{\boldsymbol{x}}\boldsymbol{u} : k_B\theta\int_{S^{d-1}} \boldsymbol{n}\otimes\nabla_{\boldsymbol{n}} f\,d\boldsymbol{n}\,d\boldsymbol{x} \overset{(13),(6)}{=} \int_\Omega \nabla_{\boldsymbol{x}}\boldsymbol{u} : \sigma\,d\boldsymbol{x}.\end{aligned}$$

The contribution of rotational diffusion leads to

$$\begin{aligned} I_{rd} &= \int_\Omega \int_{S^2} \Big(k_B\theta(1+\ln f) + U(\boldsymbol{x})\Big) D_r \Delta_{\boldsymbol{n}} f \, d\boldsymbol{n} d\boldsymbol{x} \\ &= -\frac{(k_B\theta)^2}{\zeta_r} \int_\Omega \int_{S^{d-1}} |\nabla_{\boldsymbol{n}} \ln f|^2 f \, d\boldsymbol{n} d\boldsymbol{x} \,. \end{aligned}$$

The last term in (5), modeling the effect of translational friction and translational diffusion, contributes

$$\begin{aligned} I_{tdf} &= \int_\Omega \int_{S^{d-1}} \Big(k_B\theta(1+\ln f) + U(\boldsymbol{x})\Big) D_\perp \nabla_{\boldsymbol{x}} \cdot (I + \boldsymbol{n}\otimes\boldsymbol{n}) \Big(\nabla_{\boldsymbol{x}} f + \frac{f}{k_B\theta}\nabla_{\boldsymbol{x}} U\Big) \\ &= -\frac{(k_B\theta)^2}{\zeta_\perp} \int_{S^{d-1}} \int_\Omega \nabla_{\boldsymbol{x}} \left(\ln f + \frac{1}{k_B\theta} U\right) \cdot (I + \boldsymbol{n}\otimes\boldsymbol{n}) f \nabla_{\boldsymbol{x}} \left(\ln f + \frac{1}{k_B\theta} U\right) \end{aligned}$$

Combining these terms together yields

$$\begin{aligned} &\partial_t A[f] + D_r k_B\theta \int_\Omega \int_{S^{d-1}} f |\nabla_{\boldsymbol{n}} \ln f|^2 d\boldsymbol{n} d\boldsymbol{x} \\ &+ D_\perp k_B\theta \int_\Omega \int_{S^{d-1}} \nabla_{\boldsymbol{x}} \big(\ln f + \frac{1}{k_B\theta} U\big) \cdot \big(I + \boldsymbol{n}\otimes\boldsymbol{n}\big) \nabla_{\boldsymbol{x}} \big(\ln f + \frac{1}{k_B\theta} U\big) d\boldsymbol{n} d\boldsymbol{x} \\ &= \int_\Omega \nabla_{\boldsymbol{x}} \boldsymbol{u} : \sigma d\boldsymbol{x} + \int_\Omega m_0 g \boldsymbol{e}_3 \left(\int_{S^{d-1}} f d\boldsymbol{n}\right) \cdot \boldsymbol{u} d\boldsymbol{x} \end{aligned} \tag{14}$$

We note that the second and third term capture dissipative mechanisms due to the Brownian motions, while the last two terms capture the work done by the microstructure on the fluid.

Next, we multiply the Navier-Stokes equation (8) by $\boldsymbol{u}$ and integrate over Ω to obtain the balance of the kinetic energy

$$\begin{aligned} &\frac{d}{dt} \int_\Omega \frac{1}{2} \rho_f |\boldsymbol{u}|^2 d\boldsymbol{x} + \mu \int_\Omega \nabla_{\boldsymbol{x}} \boldsymbol{u} : \nabla_{\boldsymbol{x}} \boldsymbol{u} \, d\boldsymbol{x} \\ &\qquad = -\int_\Omega \nabla_{\boldsymbol{x}} \boldsymbol{u} : \sigma \, d\boldsymbol{x} - \int_\Omega \boldsymbol{u} \cdot m_0 g \boldsymbol{e}_3 \left(\int_{S^{d-1}} f d\boldsymbol{n}\right) d\boldsymbol{x} \,. \end{aligned} \tag{15}$$

Combining (14) and (15) leads to the balance of total energy.

$$E[\boldsymbol{u}, f] = \int_\Omega \left(\frac{1}{2}\rho_f |\boldsymbol{u}|^2 + \int_{S^{d-1}} \Big((k_B\theta) f \ln f + f U(\boldsymbol{x})\Big) d\boldsymbol{n}\right) d\boldsymbol{x} \tag{16}$$

In particular, it follows that the total energy dissipates and the dissipation is due to the Brownian motions combined with the viscous dissipation of the solvent.

Non-dimensionalization. For the non-dimensionalization the units of mass, length and time are denoted by M, L and T and we monitor the dependence on the number of particles N. We list the dimensions of some terms that appear in the equations: The quantity $k_B\theta$ has dimensions of energy $\left[\frac{ML^2}{T^2}\right]$; the translational diffusion $D_\perp = \frac{k_B\theta}{\zeta_\perp}$ dimensions $\left[\frac{L^2}{T}\right]$ while the rotational diffusion $D_r = \frac{k_B\theta}{\zeta_r}$ has dimensions $\left[\frac{1}{T}\right]$; the number density f will have dimensions of number of particles / volume $\left[\frac{N}{L^3}\right]$; finally, the elastic stress of the microstructure $\sigma \sim (k_B\theta) f$ dimensions of $\left[\frac{MN}{LT^2}\right]$.

Now consider a change of scale of the form

$$t = T\hat{t},\ \boldsymbol{x} = X\hat{\boldsymbol{x}},\ \boldsymbol{u} = \frac{X}{T}\hat{\boldsymbol{u}},\ f = \frac{N}{V}\hat{f},\ p = \frac{\mu}{T}\hat{p},\ \sigma = (k_B\theta)\frac{N}{V}\hat{\sigma}. \tag{17}$$

where we used two length scales: a length scale X that will be selected in the course of the non-dimensionalization process, and a length scale L standing for the size of the macroscopic domain and entering only through the volume occupied by the suspension $V = O(L^3)$.

In these new units the Smoluchowski equation takes the form

$$\begin{aligned}&\partial_{\hat{t}}\hat{f} + \nabla_{\hat{\boldsymbol{x}}}\cdot\left(\hat{\boldsymbol{u}}\hat{f}\right) + \nabla_{\boldsymbol{n}}\cdot\left(P_{\boldsymbol{n}^\perp}\nabla_{\hat{\boldsymbol{x}}}\hat{\boldsymbol{u}}\boldsymbol{n}\hat{f}\right) = TD_r\Delta_{\boldsymbol{n}}\hat{f}\\ &+\frac{T}{X^2}D_\perp\nabla_{\hat{\boldsymbol{x}}}\cdot\left(I+\boldsymbol{n}\otimes\boldsymbol{n}\right)\nabla_{\hat{\boldsymbol{x}}}\hat{f} + \frac{D_\perp}{X}T\frac{m_0 g}{k_B\theta}\nabla_{\hat{\boldsymbol{x}}}\cdot\left(\left(I+\boldsymbol{n}\otimes\boldsymbol{n}\right)\boldsymbol{e}_3\hat{f}\right)\end{aligned} \tag{18}$$

while the elastic stress tensor (6) and the momentum equation, respectively, become

$$\hat{\sigma} = \int_{S^{d-1}}\left(d\boldsymbol{n}\otimes\boldsymbol{n} - I\right)\hat{f}d\boldsymbol{n}, \tag{19}$$

$$\begin{aligned}&\frac{X^2}{T\mu}\rho_f\left[\partial_{\hat{t}}\hat{\boldsymbol{u}} + \left(\hat{\boldsymbol{u}}\cdot\nabla_{\hat{\boldsymbol{x}}}\right)\hat{\boldsymbol{u}}\right]\\ &= \Delta_{\hat{\boldsymbol{x}}}\hat{\boldsymbol{u}} - \nabla_{\hat{\boldsymbol{x}}}\hat{p} + \frac{XT}{\mu}\frac{k_B\theta}{X}\frac{N}{V}\nabla_{\hat{\boldsymbol{x}}}\cdot\hat{\sigma} - \frac{N}{V}m_0 g\frac{XT}{\mu}\left(\int_{S^{d-1}}\hat{f}\,d\boldsymbol{n}\right)\boldsymbol{e}_3.\end{aligned} \tag{20}$$

The time scale T is an observational time scale (linked to the Deborah number) that will be selected later. The ratio X/T is fixed at this point to be the velocity of sedimentation

$$\frac{X}{T} = \frac{m_0 g}{\zeta_\perp} =: v_{sed}, \tag{21}$$

i.e. the velocity scale is proportional to the motion of a single rod falling due to gravity in a friction dominated flow.

A review of the Navier-Stokes equation indicates that there are three dimensionless numbers at play: (a) A Reynolds number based on the velocity $X/T = v_{sed}$

$$Re := \frac{Xv_{sed}}{\frac{\mu}{\rho_f}} = \rho_f\frac{X^2}{T\mu}. \tag{22}$$

(b) A dimensionless number Γ describing the ratio of elastic over viscous stresses at the fluid,

$$\Gamma := \frac{XT}{\mu}\frac{k_B\theta}{X}\frac{N}{V} = \left(\frac{X^2\rho_f}{T\mu}\right)\left(\frac{N}{V}\frac{k_B\theta}{\rho_f\left(\frac{X}{T}\right)^2}\right) = \frac{\text{inertial}}{\text{viscous}}\quad\frac{\text{elastic}}{\text{inertial}} \tag{23}$$

(c) A dimensionless number δ describing the ratio between buoyancy forces and viscous stresses,

$$\delta := \frac{N}{V}m_0 g\frac{XT}{\mu} = \left(\frac{X^2\rho_f}{T\mu}\right)\left(\frac{Nm_0 g}{V\rho_f\frac{X}{T^2}}\right) = \frac{\text{inertial}}{\text{viscous}}\quad\frac{\text{buoyancy}}{\text{inertial}} \tag{24}$$

Note that $V\rho_f v_{sed}^2 = V\rho_f\left(\frac{X}{T}\right)^2$ is the total kinetic energy of the sedimenting solution, while $Nk_B\theta$ is the total elastic energy of entropic origin of the microstructure. Hence, the last term in (23) is a ratio of elastic over inertial forces. The term $V\rho_f\frac{X}{T^2}$ is the inertial force of the solution at the selected length and time scales, while $Nm_0 g$ stands for the total buoyancy force. Hence, the last term in (24) stands for the ratio of buoyancy over inertial forces, and in

the usual practice of fluid mechanics it will be denoted as $\frac{1}{Fr}$ where Fr is a Froude number. In summary, we have two dimensionless numbers:

$$\delta = Re\frac{1}{Fr}\,, \tag{25}$$

the ratio of buoyancy over viscous stresses, and

$$\gamma := \frac{\Gamma}{\delta} = \frac{k_B\theta}{Xm_0g}\,, \tag{26}$$

which stands for the ratio of elastic over buoyancy forces. The non-dimensional form of the momentum equation then reads

$$Re\left(\partial_{\hat{t}}\hat{\boldsymbol{u}} + \left(\hat{\boldsymbol{u}}\cdot\nabla_{\hat{\boldsymbol{x}}}\right)\hat{\boldsymbol{u}}\right) = \Delta_{\hat{\boldsymbol{x}}}\hat{\boldsymbol{u}} - \nabla_{\hat{\boldsymbol{x}}}\hat{p} + \delta\gamma\nabla_{\hat{\boldsymbol{x}}}\cdot\sigma - \delta\left(\int_{S^{d-1}}\hat{f}\,d\boldsymbol{n}\right)\boldsymbol{e}_3. \tag{27}$$

We turn now to the transport equation (18) and introduce the Deborah number

$$De := \frac{1}{D_rT} \tag{28}$$

which as usual expresses the ratio of a stress relaxation time $\frac{1}{D_r}$ over the observational time scale T. By virtue of (26) and (21) we have $\frac{T}{X^2}D_\perp\frac{1}{\gamma} = \frac{T}{X^2}\frac{k_B\theta}{\zeta_\perp}\frac{Xm_0g}{k_B\theta} = 1$. The kinetic equation (18) is expressed as

$$\partial_{\hat{t}}\hat{f} + \nabla_{\hat{\boldsymbol{x}}}\cdot\left(\hat{\boldsymbol{u}}\hat{f}\right) + \nabla_{\boldsymbol{n}}\cdot\left(P_{\boldsymbol{n}^\perp}\nabla_{\hat{\boldsymbol{x}}}\hat{\boldsymbol{u}}\boldsymbol{n}\hat{f}\right) = \frac{1}{De}\Delta_{\boldsymbol{n}}\hat{f} + \nabla_{\hat{\boldsymbol{x}}}\cdot\left(I+\boldsymbol{n}\otimes\boldsymbol{n}\right)\left(\gamma\nabla_{\hat{\boldsymbol{x}}}\hat{f} + \boldsymbol{e}_3\hat{f}\right)$$

and depends on two dimensionless numbers: γ defined in (26) and the Deborah number De - or equivalently the observational time scale T. For simplicity we will use the notation D_r in the place of $\frac{1}{De}$.

The non-dimensional form of the equations is summarized (dropping the hats):

$$\begin{aligned}\partial_t f + \nabla_{\boldsymbol{x}}\cdot(\boldsymbol{u}f) + \nabla_{\boldsymbol{n}}\cdot(P_{\boldsymbol{n}^\perp}\nabla_{\boldsymbol{x}}\boldsymbol{u}\boldsymbol{n}f) - \nabla_{\boldsymbol{x}}\cdot\left(\left(I+\boldsymbol{n}\otimes\boldsymbol{n}\right)\boldsymbol{e}_3 f\right)&\\ = D_r\Delta_{\boldsymbol{n}}f + \gamma\nabla_{\boldsymbol{x}}\cdot\left(I+\boldsymbol{n}\otimes\boldsymbol{n}\right)\nabla_{\boldsymbol{x}}f&\end{aligned} \tag{29}$$

$$\sigma = \int_{S^{d-1}}\left(d\boldsymbol{n}\otimes\boldsymbol{n} - I\right)f\,d\boldsymbol{n} \tag{30}$$

$$Re\left(\partial_t\boldsymbol{u} + \left(\boldsymbol{u}\cdot\nabla_{\boldsymbol{x}}\right)\boldsymbol{u}\right) = \Delta_{\boldsymbol{x}}\boldsymbol{u} - \nabla_{\boldsymbol{x}}p + \delta\gamma\nabla_{\boldsymbol{x}}\cdot\sigma - \delta\left(\int_{S^{d-1}}f\,d\boldsymbol{n}\right)\boldsymbol{e}_3 \tag{31}$$

$$\nabla_{\boldsymbol{x}}\cdot\boldsymbol{u} = 0 \tag{32}$$

Shear flows. Let $\boldsymbol{x} = (x,y,z)^T$ and $\boldsymbol{u} = (u,v,w)^T$. We restrict attention to the case $\gamma = 0$, when the effect of the translational Brownian motion in (29) is ignored and as a consequence the effect of the elastic forces is negligible compared to the buoyancy forces. We consider an ansatz of a shear flow in the vertical direction:

$$\boldsymbol{u} = \begin{pmatrix}0\\0\\w(t,x)\end{pmatrix}, \quad f = f(t,x,\boldsymbol{n})\,, \quad p = -\kappa(t)z\,. \tag{33}$$

The director $\boldsymbol{n}$ in general takes values in S^2, which means that the rod-like particles are allowed to move out of the plane described by the direction of shear and the direction of gravity. For a shear flow, with $\boldsymbol{n} \in S^2$, the system (29)-(32) simplifies to

$$\begin{aligned} &\partial_t f(t,x,\boldsymbol{n}) + \nabla_{\boldsymbol{n}} \cdot \left(P_{\boldsymbol{n}^\perp}(0,0,n_1 w_x)^T f\right) - \partial_x(n_1 n_3 f) = D_r \Delta_{\boldsymbol{n}} f \\ &Re\, \partial_t w(t,x) = \partial_{xx} w + \delta \left(\bar{\rho} - \int_{S^2} f \, d\boldsymbol{n}\right). \end{aligned} \tag{34}$$

The form of the pressure in (33) is the most general consistent with the ansatz of a shear flow and $\kappa(t)$ can account for an externally applied pressure gradient. The choice $\kappa = \delta\bar{\rho}$ in (34), where $\bar{\rho}$ describes the total mass of suspended rods, provides an equilibrated flow. Under special boundary conditions (e.g. spatially periodic or prescribing the same distribution f at the boundary of Ω) we have conservation of the total density which determines

$$\bar{\rho} = \int_\Omega \int_{S^2} f(t,x,\boldsymbol{n}) d\boldsymbol{n} dx = \int_\Omega \int_{S^2} f(0,x,\boldsymbol{n}) d\boldsymbol{n} dx.$$

An even simpler system is obtained, if we consider again a shear flow (33) but restrict the director to take values in the (x,z) plane, i.e. the plane spanned by the direction of shear and the direction of gravity. (While this restriction is not natural, it turns out to be much simpler to analyze and in retrospect to provide the same form of macroscopic equations.) In this situation the shear is again $w_x = \partial_x w$ but now $\boldsymbol{n} \in S^1$, that is $\boldsymbol{n} = (\cos\theta, \sin\theta)^T$ where the angle $\theta \in [0, 2\pi]$ is measured counter-clockwise from the positive x-axis. The model for shear flow can be written in the form

$$\begin{aligned} &\partial_t f(t,x,\theta) + \partial_\theta \left(w_x \cos^2\theta f\right) - \partial_x \left(\sin\theta \cos\theta f\right) = D_r \partial_{\theta\theta} f \\ &Re\, \partial_t w(t,x) = \partial_{xx} w + \delta \left(\bar{\rho} - \int_0^{2\pi} f \, d\theta\right). \end{aligned} \tag{35}$$

We now consider numerical simulations of system (35), which resemble the basic mechanism of cluster formation that is observed in experimental studies of sedimentations of rod-like particles. Since we are interested in the process of cluster formation, we monitor the density of rod-like particles as a function of space and time. In our simplified situation this means that we monitor

$$\rho(t,x) = \int_0^{2\pi} f(t,x,\theta) d\theta. \tag{36}$$

Initially this density is set to approximately one, i.e. $\rho(x,0) = 1 + \epsilon_1(x)$ where $\epsilon_1(x)$ is a small random perturbation, see Figure 2 (left plot). The initial values of f used in the computation are constant in θ, i.e. we use $f(0,x,\theta) = (1 + \epsilon_1(x))/2\pi$. The vertical velocity component w is initially set to zero.

In Figure 2 (middle and right plot) we show $\rho(x,t)$ as computed via (36) from the numerical results of f at different times. We observe that after some time clusters of higher particle density form. In applications where we are only interested in the particle density $\rho(x,t)$ and not in a more detailed description of the particle orientation, it would be much more efficient to compute numerical solutions of mathematical models which directly describe the evolution of ρ without computing f. In this paper we describe different approaches to derive such models.

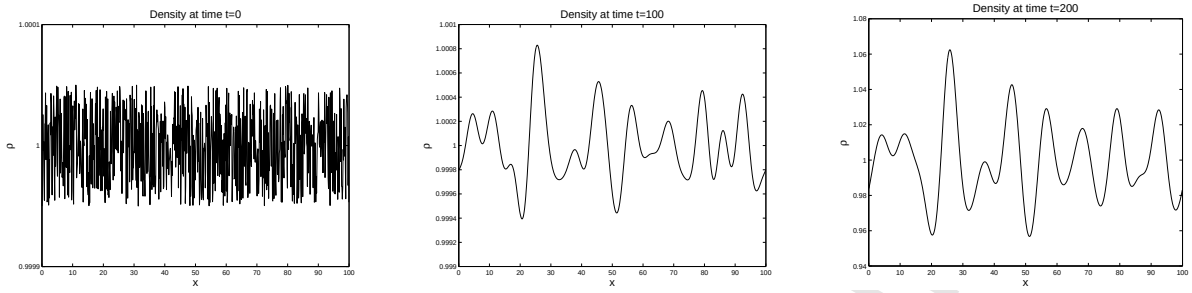

Figure 2: Numerical results for system (35).

3 Nonlinear moment closure

In this section we consider (35) and proceed to describe the evolution of a system of moments. The macroscopic density is

$$\rho(t,\boldsymbol{x}) = \int_{S^1} f(t,\boldsymbol{x},\boldsymbol{n})\, d\boldsymbol{n}.$$

We use as basis for the moments the eigenfunctions of the Laplace-Beltrami operator $\partial_{\theta\theta}$ on the circle S^1. These are the functions 1, and $\cos n\theta$, $\sin n\theta$, $n = 1, 2, 3, \ldots$. Since the rods are identical under the reflection $\theta \to -\theta$ only the even eigenfunctions will play a role.

First we derive a nonlinear system of equations for the zero-th order moment ρ and the second order moments s and c, defined via the relations

$$\begin{aligned}
\rho(t,x) &:= \int_0^{2\pi} f(t,x,\theta)\, d\theta \\
c(t,x) &:= \frac{1}{2}\int_0^{2\pi} f(t,x,\theta)\cos(2\theta)\, d\theta \\
s(t,x) &:= \frac{1}{2}\int_0^{2\pi} f(t,x,\theta)\sin(2\theta)\, d\theta.
\end{aligned}$$

We will close the system by neglecting the moments of order higher than 2. This closure is based on the premise that higher moments will experience faster decay, as they correspond to a larger eigenvalue of the Laplace-Beltrami operator. The validity of this hypothesis will be tested numerically.

In our derivation we consider the different terms of the first equation in (35) separately, using the notation

$$\partial_t f = \underbrace{-\partial_\theta\left(w_x \cos^2\theta\, f\right)}_{[1]} + \underbrace{\partial_x\left(\sin\theta\cos\theta f\right)}_{[2]} + \underbrace{D_r\partial_{\theta\theta} f}_{[3]}. \tag{37}$$

The evolution equation for ρ is obtained by integrating (37) over S^1. Note that there is no contribution from [1] and [3], and

$$\begin{aligned}
\partial_t\rho &= \int_0^{2\pi} \partial_t f\, d\theta \\
&= \int_0^{2\pi} \partial_x\left(\sin\theta\cos\theta f\right)\, d\theta = \partial_x s.
\end{aligned}$$

To obtain the evolution equation for c, we compute

$$\partial_t c = \frac{1}{2}\int_0^{2\pi} \cos(2\theta)\partial_t f \, d\theta.$$

We separately consider the different contributions from the right hand side of (37). contribution from [1]:

$$\begin{aligned}
-\frac{1}{2}\int_0^{2\pi} \cos(2\theta)\partial_\theta \left(w_x \cos^2\theta f\right) \, d\theta &= -\frac{1}{2} w_x \int_0^{2\pi} \cos(2\theta)\partial_\theta \left(\frac{1}{2}(1+\cos 2\theta) f\right) \, d\theta \\
&= -w_x \int_0^{2\pi} \sin(2\theta)\frac{1}{2}(1+\cos(2\theta) f \, d\theta \\
&= -w_x s - \frac{1}{4} w_x \int_0^{2\pi} \sin(4\theta) f \, d\theta
\end{aligned}$$

contribution from [2]:

$$\begin{aligned}
\frac{1}{2}\int_0^{2\pi} \cos(2\theta)\partial_x \left(\sin\theta\cos\theta \, f\right) \, d\theta &= \frac{1}{4}\int_0^{2\pi} \cos(2\theta)\sin(2\theta)\partial_x f \, d\theta \\
&= \frac{1}{8}\int_0^{2\pi} \sin(4\theta)\partial_x f \, d\theta
\end{aligned}$$

contribution from [3]:

$$\begin{aligned}
\frac{1}{2}\int_0^{2\pi} \cos(2\theta) D_r \partial_{\theta\theta} f \, d\theta &= D_r \int_0^{2\pi} \sin(2\theta)\partial_\theta f \, d\theta \\
&= -2D_r \int_0^{2\pi} \cos(2\theta) f \, d\theta \\
&= -4D_r c
\end{aligned}$$

Now we neglect higher order moments, i.e. terms that involve integrals of the form $\int_0^{2\pi} \sin(4\theta) f \, d\theta$ and $\int_0^{2\pi} \cos(4\theta) f \, d\theta$. Under this assumption, the evolution equation for c has the form

$$\partial_t c = -w_x s - 4D_r c.$$

Similarly we can derive an evolution equation for s. The complete nonlinear moment closure system reads

$$\partial_t \rho = \partial_x s \tag{38}$$

$$\partial_t c = -w_x s - 4D_r c \tag{39}$$

$$\partial_t s = \frac{1}{8}\partial_x \rho + w_x c + \frac{1}{4} w_x \rho - 4D_r s \tag{40}$$

$$Re\partial_t w = \partial_{xx} w + \delta\left(\bar{\rho} - \rho\right). \tag{41}$$

4 The quasi-dynamic approximation

In [8], we derived various systems of evolution equations describing the macroscopic behavior of the system (34) for intermediate and long times. We considered rectilinear flows in the direction of gravity with the rod orientations taking values on the sphere S^2 and derived the

so called quasi-dynamic approximation (*cf* [8]). When we restrict our analysis to a shear flow (33) and set $D_r = 1$ we obtain the system consisting of an advection-diffusion equation coupled to a diffusion equation,

$$\begin{aligned} \partial_t \rho(t,x) &= \frac{1}{30}\partial_x \left[\frac{42^2}{42^2 + 46 w_x^2} \left(\rho w_x + \frac{1}{3}\partial_x \rho \right) \right] \\ Re\, \partial_t w(t,x) &= \partial_{xx} w + \delta\left(\bar{\rho} - \rho\right). \end{aligned} \tag{42}$$

This model belongs to the class of flux-limited Keller-Segel systems and enjoys gradient-flow structure (see [8]). The derivation of (42) is quite technical due to the complex form of the moment equations (and their closures) reflecting the structure of harmonic polynomials in dimension $d > 2$.

To shed some light on the derivation of (42), we consider the simplified shear flow model (35), where now the rigid-rods are constrained to move in-plane, $\boldsymbol{n} \in S^1$, and present a derivation of the quasi-dynamic approximation. The idea behind the quasi-dynamic approximation is that the transient dynamics (39)-(40) of the second order moments c and s is replaced by its equilibrium response, i.e. by

$$\begin{aligned} 4D_r c + w_x s &= 0 \\ -\frac{1}{8}\partial_x \rho - \frac{1}{4} w_x \rho - w_x c + 4 D_r s &= 0. \end{aligned} \tag{43}$$

System (43) can be solved for s, to obtain

$$s = \frac{D_r w_x \rho + \frac{1}{2} D_r \partial_x \rho}{16 D_r^2 + w_x^2}. \tag{44}$$

Inserting (44) into (38), we obtain the quasi-dynamic approximation

$$\begin{aligned} \partial_t \rho &= \partial_x \left(\frac{D_r w_x}{16 D_r^2 + w_x^2} \rho \right) + \frac{1}{2} D_r \partial_x \left(\frac{1}{16 D_r^2 + w_x^2} \partial_x \rho \right) \\ Re \partial_t w &= \partial_{xx} w + \delta\left(\bar{\rho} - \rho\right). \end{aligned} \tag{45}$$

For the special case $D_r = 1$ it gives

$$\begin{aligned} \partial_t \rho &= \partial_x \left(\frac{1}{16 + w_x^2} \left(w_x \rho + \frac{1}{2} \partial_x \rho \right) \right) \\ Re \partial_t w &= \partial_{xx} w + \delta\left(\bar{\rho} - \rho\right). \end{aligned} \tag{46}$$

A comparison of (46) with (42) shows that we obtain the same general structure of a flux-limited Keller-Segel model. The simplification, which restricts the director to S^1, just leads to different constants.

5 The diffusive scaling

The diffusive scaling provides another approach for obtaining a macroscopic evolution equation for ρ. Here we present a direct derivation of the diffusive scaling for the simplified shear flow model (35), where we assume that the director f only takes values on S^1. Again we restrict our considerations to the case $D_r = 1$.

We consider (35) and rescale the model in the diffusive scale, i.e.

$$x = \frac{1}{\delta}\hat{x},\ t = \frac{1}{\delta^2}\hat{t},\ \boldsymbol{u} = \hat{\boldsymbol{u}}.$$

The scaled equations (dropping the hats and for $D_r = 1$) have the form

$$\begin{aligned} &\delta^2\,\partial_t f(t,x,\theta) + \delta\,\partial_\theta\left(w_x\cos^2\theta f\right) - \delta\partial_x\left(\sin\theta\cos\theta f\right) = \partial_{\theta\theta} f \\ &Re\,\delta^2\,\partial_t w(t,x) = \delta^2\,\partial_{xx} w + \delta\left(\bar{\rho} - \int_0^{2\pi} f\,d\theta\right). \end{aligned} \tag{47}$$

Now we introduce the ansatz

$$\begin{aligned} f(t,x,\theta) &= \delta f_0 + \delta^2 f_1 + \dots \\ \boldsymbol{u} = \boldsymbol{u}_0 + \delta\boldsymbol{u}_1 + \dots &= \begin{pmatrix} 0 \\ w_0 \end{pmatrix} + \delta\begin{pmatrix} 0 \\ w_1 \end{pmatrix} + \dots \\ \bar{\rho} &= \delta\bar{\rho}_0 + \delta^2\bar{\rho}_1 + \dots \end{aligned}$$

and obtain the relations

$$O(\delta) \qquad \partial_{\theta\theta} f_0 = 0 \tag{48}$$

$$O(\delta^2) \qquad \partial_\theta\left(w_x\cos^2\theta f_0\right) - \partial_x\left(\sin\theta\cos\theta f_0\right) = \partial_{\theta\theta} f_1 \tag{49}$$

$$Re\partial_t w_0 = \partial_{xx} w_0 + \left(\bar{\rho}_0 - \int_0^{2\pi} f_0 d\theta\right)$$

$$O(\delta^3) \qquad \partial_t f_0 + \partial_\theta\left(w_x\cos^2\theta f_1\right) - \partial_x\left(\sin\theta\cos\theta f_1\right) = \partial_{\theta\theta} f_2. \tag{50}$$

The relation (48) implies that f_0 depends at most linearly on θ. As a function on S^1, f is periodic. Thus, f_0 must be constant in θ and

$$\rho_0(t,x) = \int_0^{2\pi} f_0(t,x)d\theta = 2\pi f_0(t,x).$$

Now we integrate equation (50) over S^1. The second and the last term vanish and we obtain

$$\partial_t\rho_0 - \partial_x\int_0^{2\pi}\cos\theta\sin\theta f_1\,d\theta = 0.$$

Using integration by parts, we arrive at

$$\begin{aligned} \partial_t\rho_0 &= -\frac{1}{4}\partial_x\left(\int_0^{2\pi}\partial_{\theta\theta}\left(\cos\theta\sin\theta\right) f_1\,d\theta\right) \\ &= -\frac{1}{4}\partial_x\left(\int_0^{2\pi}\cos\theta\sin\theta\,\partial_{\theta\theta} f_1\,d\theta\right). \end{aligned}$$

Using (49), we replace $\partial_{\theta\theta} f_1$ by terms which depend on f_0 and obtain an evolution equation for ρ_0:

$$\begin{aligned} \partial_t\rho_0 &= -\frac{1}{4}\partial_x\left(\int_0^{2\pi}\cos\theta\sin\theta\left[\partial_\theta\left(w_x\cos^2\theta f_0\right) - \partial_x\left(\sin\theta\cos\theta f_0\right)\right]\,d\theta\right) \\ &= \frac{1}{4\pi}\,\partial_x\left(w_x\rho_0\int_0^{2\pi}\cos^2\theta\sin^2\theta\,d\theta\right) + \frac{1}{8\pi}\partial_x\left(\partial_x\rho_0\int_0^{2\pi}\cos^2\theta\sin^2\theta\,d\theta\right) \\ &= \frac{1}{16}\partial_x\left(w_x\rho_0\right) + \frac{1}{32}\partial_{xx}\rho_0. \end{aligned}$$

Thus, in the diffusive limit, the dynamics of the simplified shear flow problem (35) is described by the system

$$\begin{aligned} \partial_t \rho &= \frac{1}{16}\partial_x \left(w_x \rho + \frac{1}{2}\partial_x \rho \right) \\ Re\, \partial_t w &= \partial_{xx} w + (\bar{\rho} - \rho)\,. \end{aligned} \tag{51}$$

In Appendix A.2, we derive the diffusive scaling for the kinetic model (29)-(32) in the case of rectilinear flow for rigid rods where the director is allowed to take values in S^2. For shear flow and in the special case $D_r = 1$, $\gamma = 0$, the diffusive scaling of (34) leads to the model equation

$$\begin{aligned} \partial_t \rho &= \frac{1}{30}\partial_x \left(w_x \rho + \frac{1}{3}\partial_x \rho \right) \\ Re \partial_t w &= \partial_{xx} w + (\bar{\rho} - \rho)\,. \end{aligned} \tag{52}$$

Again we obtain a Keller-Segel type model. In contrast to the quasi-dynamic approximation, the diffusive scaling does not provide flux limiting.

6 Numerical simulations

In this section we show numerical simulations for shear flow, which compare the simplified shear flow model (35) with the quasi-dynamic approximation (42) and the diffusive scaling (51). In Figure 3 we show results of numerical simulations using the parameter values $D_r = \delta = Re = 1$. The initial values are set to be

$$\begin{aligned} \rho(x_k, 0) &= 1 + 10^{-4} \left(\epsilon(x_k) - \frac{1}{2} \right) \\ w(x_k, 0) &= 0, \end{aligned} \tag{53}$$

where $\epsilon(x_k)$ is a random number between 0 and 1. We impose the periodicity condition on an interval of length 100. For our test simulations we used 800 grid cells in space, thus $k = 1, \ldots, 800$. In the simulation of the full model, S^1 is discretized with 200 grid cells. We observe the formation of clusters with higher particle density.

Both the solutions predicted by the quasi-dynamic approximation as well as the solutions predicted by the diffusive limit compare very well with the solution structure obtained by the full model. Only at very late times, some differences can be observed and the quasi-dynamic approximation leads to slightly more accurate results.

Note that the model equations obtained by the quasi-dynamic approximation contain the same non-dimensional parameters as the full model. For the diffusive limit this is not the case, since the parameter δ does no longer appear in (51). Using our insight from the derivation of the diffusive model, we can nevertheless set up a simulation for values $\delta \neq 1$. In order to simulate the problem with the diffusive model, we impose periodic boundary conditions on a domain of length $\delta 100 = 20$ and consider numerical approximations for $t \leq \delta^2 2000 = 80$. Furthermore, we set initial values as described by (53) but multiplied by $1/\delta$. Finally we replaced $\bar{\rho}$ by $\bar{\rho}/\delta$ in equation (51). To compare the numerical solution of the diffusive limit system with the solution of the full model, we map the numerical solution to the interval $[0, 100]$ and multiply with δ. In Figure 4 we show simulations comparing the quasi-dynamic approximation with the full model for $\delta = 0.2$.

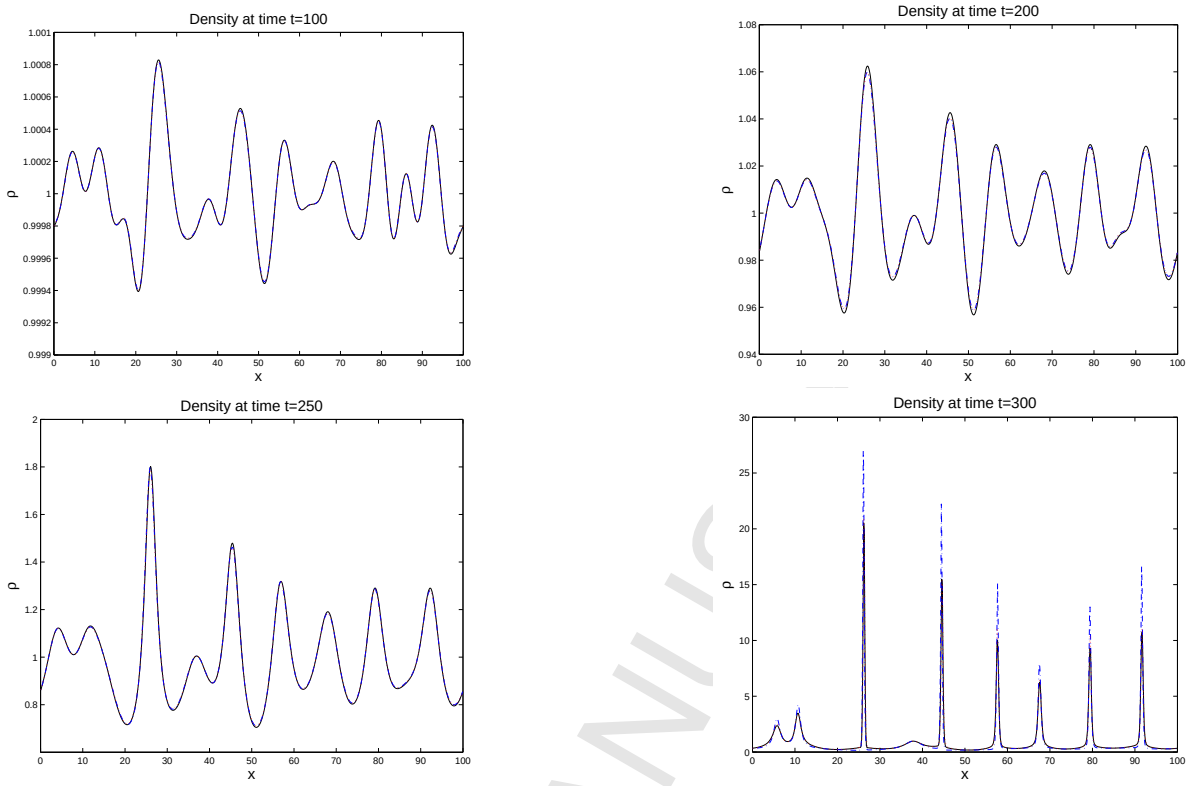

Figure 3: Comparison of the density as predicted by the full model (black solid line) with the prediction of the diffusive scaling (blue dashed-dotted line) and the quasi-dynamic approximation (red dotted line) at different times.

At later times the cluster start to merge. This coarsening behavior can be observed with all of the three models. Here a slightly better agreement is observed for the quasi-dynamic approximation.

Conclusions

Based on a simplified kinetic model, we have studied the sedimentation of rod-like particles under the influence of gravity. Linear stability shows both instability of a well stirred initial configuration as well as a wave length selection mechanism for a non-zero Reynolds number. We presented two models describing the macroscopic response of the system. One of these models, the quasi-dynamic approximation, is obtained from a moment closure system using the assumption that the evolution equation of the second order moments can be replaced by an equilibrium relation. The resulting macroscopic system has the form of a flux-limited Keller-Segel model. Another macroscopic model is obtained by taking the diffusive limit of the kinetic model. In this case we obtain a standard Keller-Segel type model. Numerical computations confirm good agreement of the predicted solution structure of both macroscopic models compared to the kinetic model. For very long times the quasi-dynamic approximation shows a better agreement with the original kinetic model.

Finally, it is interesting to note the differences of the macroscopic models depending on whether the orientation of the rod-like particles is a function on S^1 or S^2, respectively. The

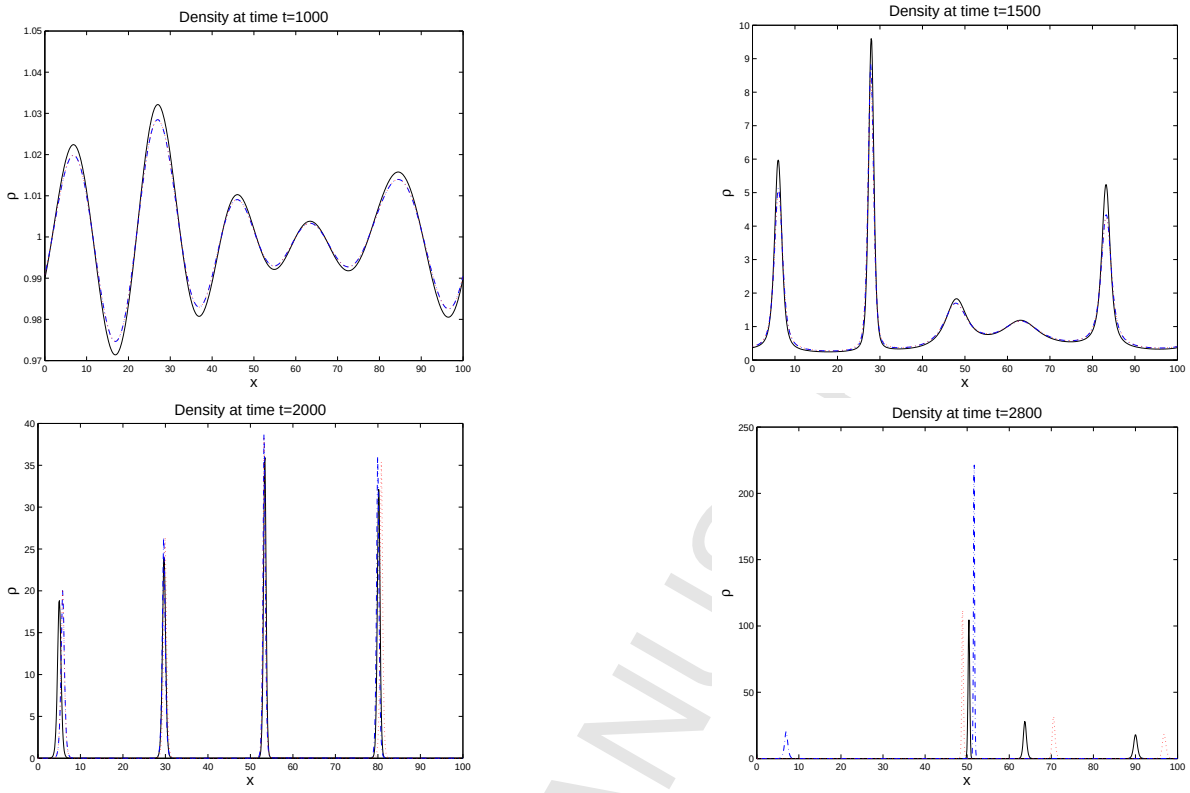

Figure 4: Comparison of the density as predicted by the full model (black solid line) with the prediction of the diffusive scaling (blue dashed-dotted line) and the quasi-dynamic approximation (red dotted line) at different times. The simulation corresponds to $\delta = 0.2$.

macroscopic models which are derived from the simplified kinetic model are less diffusive than those which are derived from the more general kinetic model.

A Appendix: Collective behavior in scaling limits

In this appendix we derive the hyperbolic and diffusive limits for the system (29)-(32). The description of collective behavior of kinetic models through hyperbolic or parabolic limits is well known in several contexts in fluid dynamics or biological transport systems (*e.g.* [3, 13, 15]). The novelty here is that the kinetic variable takes values in the sphere, which requires some special calculations detailed in this appendix.

It is expedient to view the scaling limits from the perspective of describing the aggregate behavior of a suspension. The function

$$\rho(t, \boldsymbol{x}) = \int_{S^{d-1}} f(t, \boldsymbol{x}, \boldsymbol{n}) d\boldsymbol{n}$$

measures the density of rod-like particles. Linear stability theory predicts an instability for the quiescent solution; it is then natural to calculate the aggregate response of the system in long times. To this end, we proceed to calculate the hyperbolic and diffusive limits. It turns out that the limiting behavior in the hyperbolic scaling will be described by a Boussinesq type system. For certain flows the hyperbolic scaling produces a trivial behavior, and it is then natural to

consider the diffusive scaling. Such a situation occurs for two-dimensional rectilinear flows of suspensions, where we will show that the collective behavior in the diffusive limit is described by the Keller-Segel model. The calculations below are presented for space dimension $d = 3$ and $\boldsymbol{n} \in S^2$.

A.1 The hyperbolic scaling

We first rescale the model (29)-(32) in the *hyperbolic scaling*,

$$\boldsymbol{x} = \frac{1}{\delta}\hat{\boldsymbol{x}},\ t = \frac{1}{\delta}\hat{t},\ \boldsymbol{u} = \hat{\boldsymbol{u}},\ p = \hat{p}.$$

The scaled equations (after dropping the hats) are

$$\begin{aligned} \delta\partial_t f + \delta\boldsymbol{u}\cdot\nabla_{\boldsymbol{x}} f - \delta D(\boldsymbol{n})\boldsymbol{e}_3\cdot\nabla_{\boldsymbol{x}} f + \delta\nabla_{\boldsymbol{n}}\cdot(P_{\boldsymbol{n}^\perp}\nabla_{\boldsymbol{x}}\boldsymbol{u}\boldsymbol{n} f) \\ = D_r\Delta_{\boldsymbol{n}} f + \delta^2\gamma\nabla_{\boldsymbol{x}}\cdot D(\boldsymbol{n})\nabla_{\boldsymbol{x}} f \\ Re\,\delta\,(\partial_t\boldsymbol{u} + (\boldsymbol{u}\cdot\nabla_{\boldsymbol{x}})\,\boldsymbol{u}) - \delta^2\Delta_{\boldsymbol{x}}\boldsymbol{u} + \delta\nabla_{\boldsymbol{x}} p - \delta^2\gamma\nabla_{\boldsymbol{x}}\cdot\sigma = -\delta\Big(\int_{S^2} f d\boldsymbol{n}\Big)\boldsymbol{e}_3 \\ \delta\nabla_{\boldsymbol{x}}\cdot\boldsymbol{u} = 0, \end{aligned} \tag{54}$$

where $D(\boldsymbol{n}) = I + \boldsymbol{n}\otimes\boldsymbol{n}$.

We introduce the ansatz

$$\begin{aligned} f &= f_0 + \delta f_1 + \dots \\ \boldsymbol{u} &= \boldsymbol{u}_0 + \delta\boldsymbol{u}_1 + \dots \\ p &= p_0 + \delta p_1 + \dots \end{aligned}$$

to the system (54) and obtain equations for the various orders of the expansion:

$$O(1) \qquad \Delta_{\boldsymbol{n}} f_0 = 0 \tag{55}$$

$$O(\delta) \qquad \partial_t f_0 + \boldsymbol{u}_0\cdot\nabla_{\boldsymbol{x}} f_0 - D(\boldsymbol{n})\boldsymbol{e}_3\cdot\nabla_{\boldsymbol{x}} f_0 + \nabla_{\boldsymbol{n}}\cdot(P_{\boldsymbol{n}^\perp}\nabla_{\boldsymbol{x}}\boldsymbol{u}_0\boldsymbol{n} f_0) = \Delta_{\boldsymbol{n}} f_1 \tag{56}$$

$$O(\delta) \qquad Re\ (\partial_t\boldsymbol{u}_0 + (\boldsymbol{u}_0\cdot\nabla_{\boldsymbol{x}})\,\boldsymbol{u}_0) + \nabla_{\boldsymbol{x}} p_0 = -\Big(\int_{S^2} f_0 d\boldsymbol{n}\Big)\boldsymbol{e}_3$$

$$O(\delta) \qquad \nabla_{\boldsymbol{x}}\cdot\boldsymbol{u}_0 = 0$$

It follows from (55) that f_0 is independent of $\boldsymbol{n}$ and thus

$$f_0(t,\boldsymbol{x},\boldsymbol{n}) = \frac{1}{4\pi}\int_{S^2} f_0 d\boldsymbol{n} = \frac{1}{4\pi}\rho_0(t,\boldsymbol{x})$$

Then integrating (56) over the sphere, we deduce that $\rho_0 = \int_{S^2} f_0 d\boldsymbol{n}$ and $\boldsymbol{u}_0$ satisfy the Boussinesq system

$$\begin{aligned} \partial_t\rho_0 + \nabla_{\boldsymbol{x}}\cdot\Big(\boldsymbol{u}_0\rho_0 - \big(\frac{1}{4\pi}\int_{S^2} D(\boldsymbol{n})d\boldsymbol{n}\big)\boldsymbol{e}_3\rho_0\Big) = 0 \\ Re\ (\partial_t\boldsymbol{u}_0 + (\boldsymbol{u}_0\cdot\nabla_{\boldsymbol{x}})\,\boldsymbol{u}_0) + \nabla_{\boldsymbol{x}} p_0 = -\rho_0\boldsymbol{e}_3 \\ \nabla_{\boldsymbol{x}}\cdot\boldsymbol{u}_0 = 0. \end{aligned} \tag{57}$$

A.2 The diffusive scaling

Next, we confine to rectilinear flows with a vertical velocity field obeying the ansatz

$$\boldsymbol{u}(t,x,y) = (0,0,w(t,x,y))^T\,, \quad f = f(t,x,y,\boldsymbol{n}) \tag{58}$$

depending only on the horizontal variables (x,y). The flow cross section is the domain D and we assume that the boundary conditions are either periodic or no-slip. This restriction to the two-dimensional case is motivated by experimental observations of long clusters with higher particle density. We note that for this ansatz the nonlinear transport terms $\boldsymbol{u}\cdot\nabla f$ and $(\boldsymbol{u}\cdot\nabla)\boldsymbol{u}$ drop out and the pressure must be of the form $p = -\kappa(t)z$. One checks that under the ansatz (58) the system (57) reduces to the trivial problem

$$\partial_t\rho_0 = 0, \quad Re\,\partial_t w_0 = (\bar\rho - \rho_0)\,, \quad p_0 = -\bar\rho z$$

which can be easily solved in terms of the initial data.

The objective then becomes to calculate the next order correction in the diffusive scale. We return to (29)-(32) and introduce the *diffusive scaling*, i.e.

$$\boldsymbol{x} = \frac{1}{\delta}\hat{\boldsymbol{x}},\ t = \frac{1}{\delta^2}\hat t,\ \boldsymbol{u} = \hat{\boldsymbol{u}},\ p = \hat p,\ f = \hat f. \tag{59}$$

The scaled equations (after dropping the hats) have the form

$$\begin{aligned}
\delta^2\partial_t f - \delta D(\boldsymbol{n})\boldsymbol{e}_3\cdot\nabla_{\boldsymbol{x}} f + \delta\nabla_{\boldsymbol{n}}\cdot(P_{\boldsymbol{n}^\perp}\nabla_{\boldsymbol{x}}\boldsymbol{u}\boldsymbol{n}f) &= D_r\Delta_{\boldsymbol{n}} f + \delta^2\gamma\nabla_{\boldsymbol{x}}\cdot D(\boldsymbol{n})\nabla_{\boldsymbol{x}} f\\
\delta^2\,Re\,\partial_t\boldsymbol{u} + \delta\nabla_{\boldsymbol{x}} p &= \delta^2\Delta_{\boldsymbol{x}}\boldsymbol{u} + \delta^2\gamma\nabla_{\boldsymbol{x}}\cdot\sigma - \delta\Big(\int_{S^2} f d\boldsymbol{n}\Big)\boldsymbol{e}_3\\
\delta\nabla_{\boldsymbol{x}}\cdot\boldsymbol{u} &= 0
\end{aligned}$$

We introduce the ansatz

$$\begin{aligned}
f(t,x,y,\boldsymbol{n}) &= \delta f_0 + \delta^2 f_1 + \dots\\
\boldsymbol{u}(t,x,y) &= \boldsymbol{u}_0 + \delta\boldsymbol{u}_1 + \dots = \begin{pmatrix}0\\0\\w_0\end{pmatrix} + \delta\begin{pmatrix}0\\0\\w_1\end{pmatrix} + \dots\\
p &= \delta p_0 + \delta^2 p_1 + \dots
\end{aligned} \tag{60}$$

to the above system and collect the terms of the same order,

$$\begin{aligned}
O(\delta)\qquad & \Delta_{\boldsymbol{n}} f_0 = 0 && (61)\\
O(\delta^2)\qquad & -D(\boldsymbol{n})\boldsymbol{e}_3\cdot\nabla_{\boldsymbol{x}} f_0 + \nabla_{\boldsymbol{n}}\cdot(P_{\boldsymbol{n}^\perp}\nabla_{\boldsymbol{x}}\boldsymbol{u}_0\boldsymbol{n}f_0) = D_r\Delta_{\boldsymbol{n}} f_1 && (62)\\
O(\delta^3)\qquad & \partial_t f_0 - D(\boldsymbol{n})\boldsymbol{e}_3\cdot\nabla_{\boldsymbol{x}} f_1 + \nabla_{\boldsymbol{n}}\cdot\big(P_{\boldsymbol{n}^\perp}\big(\nabla_{\boldsymbol{x}}\boldsymbol{u}_1\boldsymbol{n}f_0 + \nabla_{\boldsymbol{x}}\boldsymbol{u}_0\boldsymbol{n}f_1\big)\big)\\
& \qquad = D_r\Delta_{\boldsymbol{n}} f_2 + \gamma\nabla_{\boldsymbol{x}}\cdot D(\boldsymbol{n})\nabla_{\boldsymbol{x}} f_0 && (63)
\end{aligned}$$

The same procedure applied to the Stokes system yields

$$\begin{aligned}
O(\delta)\qquad & \nabla_{\boldsymbol{x}}\cdot\boldsymbol{u}_0 = 0\\
O(\delta^2)\qquad & \partial_t\boldsymbol{u}_0 + \nabla_{\boldsymbol{x}} p_0 = \Delta_{\boldsymbol{x}}\boldsymbol{u}_0 - \left(\int_{S^2} f_0 d\boldsymbol{n}\right)\boldsymbol{e}_3 && (64)
\end{aligned}$$

We proceed to derive an evolution equation for ρ_0 and w_0. In order to do this, we first summarise a few tools. Recall that $\boldsymbol{n} \in S^2$ has the form

$$\boldsymbol{n} = \begin{pmatrix} \sin\theta\cos\phi \\ \sin\theta\sin\phi \\ \cos\theta \end{pmatrix}, \quad 0 \le \theta < \pi,\, 0 \le \phi < 2\pi.$$

Furthermore, recall that the components of the tensor $3\boldsymbol{n}\otimes\boldsymbol{n} - \mathrm{I}$ are the surface spherical harmonics of order 2. This means, they are harmonic polynomials on $\mathbb{R}^3$ of order 2, restricted to S^2. The surface spherical harmonics are eigenfunctions of the Laplacian on S^2 with corresponding eigenvalue $-\ell(\ell+1)$, where ℓ is the order [1, App. E]. Hence

$$\triangle_{\boldsymbol{n}}(3\,n_i\,n_j - \delta_{ij}) \;=\; -6\,(3\,n_i\,n_j - \delta_{ij}). \tag{65}$$

Finally, note that for any 3×3 matrix κ, the equation

$$\nabla_{\boldsymbol{n}} \cdot (P_{\boldsymbol{n}^\perp}\kappa\boldsymbol{n}) = \mathrm{tr}\;\kappa - 3\boldsymbol{n}\cdot\kappa\boldsymbol{n}, \tag{66}$$

holds, where tr stands for the trace operator. Also, using symmetries of S^2, we obtain the formula

$$\frac{1}{4\pi}\int_{S^2} \boldsymbol{n}\otimes\boldsymbol{n}d\boldsymbol{n} = \tfrac{1}{3}I. \tag{67}$$

Now we are ready to derive an evolution equation for ρ_0. Equation (61) implies that f_0 is independent on $\boldsymbol{n}$, that is

$$f_0 = \frac{1}{4\pi}\int_{S^2} f_0 d\boldsymbol{n} = \frac{1}{4\pi}\rho_0(t,x,y)$$

Next, integration of (63) over the sphere and use of (67) and the fact that $\boldsymbol{e}_3\cdot\nabla_x f_1 = 0$ for our ansatz gives that ρ_0 satisfies

$$\partial_t\rho_0 = \nabla_{\boldsymbol{x}}\cdot\underbrace{\int_{S^2}\left(D(\boldsymbol{n}) - \frac{1}{4\pi}\int_{S^2} D(\boldsymbol{n})d\boldsymbol{n}\right)\boldsymbol{e}_3 f_1\, d\boldsymbol{n}}_{=:I_1} + \gamma\nabla_{\boldsymbol{x}}\cdot\underbrace{\frac{1}{4\pi}\int_{S^2} D(\boldsymbol{n})d\boldsymbol{n}}_{=:I_2}\nabla_{\boldsymbol{x}}\rho_0 \tag{68}$$

where the terms I_1 and I_2 are computed in terms of f_1 solving (62) for $f_0 = \frac{1}{4\pi}\rho_0$.

It remains to compute the terms I_1 and I_2. Observe now that we have the identities:

$$\begin{aligned} \int_{S^2}(\boldsymbol{n}\otimes\boldsymbol{n} - \frac{1}{3}I)d\boldsymbol{n} &\overset{(65)}{=} -\frac{1}{6}\int_{S^2}\triangle_{\boldsymbol{n}}(\boldsymbol{n}\otimes\boldsymbol{n} - \frac{1}{3}I)d\boldsymbol{n} = 0 \\ I_2 := \frac{1}{4\pi}\int_{S^2} D(\boldsymbol{n})d\boldsymbol{n} &= \frac{1}{4\pi}\int_{S^2}(\boldsymbol{n}\otimes\boldsymbol{n} + I)d\boldsymbol{n} = \frac{4}{3}I \\ D(\boldsymbol{n}) - \frac{1}{4\pi}\int_{S^2} D(\boldsymbol{n})d\boldsymbol{n} &= \boldsymbol{n}\otimes\boldsymbol{n} - \frac{1}{3}I \end{aligned} \tag{69}$$

These, in conjunction with (61), (62) and (66), imply that f_1 satisfies

$$\begin{aligned} \Delta_{\boldsymbol{n}} f_1 &= -\big(D(\boldsymbol{n}) - \frac{1}{4\pi}\int_{S^2} D(\boldsymbol{n})d\boldsymbol{n}\big)\boldsymbol{e}_3\cdot\frac{1}{4\pi}\nabla_{\boldsymbol{x}}\rho_0 + \frac{1}{4\pi}\nabla_{\boldsymbol{n}}\cdot(P_{\boldsymbol{n}^\perp}\nabla_{\boldsymbol{x}}\boldsymbol{u}_0\boldsymbol{n})\,\rho_0 \\ &= -\big(\boldsymbol{n}\otimes\boldsymbol{n} - \frac{1}{3}I\big)\boldsymbol{e}_3\cdot\frac{1}{4\pi}\nabla_{\boldsymbol{x}}\rho_0 - \frac{3}{4\pi}\rho_0(\boldsymbol{n}\cdot\nabla_{\boldsymbol{x}}\boldsymbol{u}_0\boldsymbol{n}). \end{aligned} \tag{70}$$

Next, we compute I_1

$$\begin{aligned}
I_1 &:= \int_{S^2} \left(D(\boldsymbol{n}) - \frac{1}{4\pi} \int_{S^2} D(\boldsymbol{n}) d\boldsymbol{n} \right) \boldsymbol{e}_3 f_1 \, d\boldsymbol{n} \\
&= \int_{S^2} (\boldsymbol{n} \otimes \boldsymbol{n} - \frac{1}{3} I) \boldsymbol{e}_3 f_1 d\boldsymbol{n} \\
&\overset{(65)}{=} -\frac{1}{6} \int_{S^2} \triangle_{\boldsymbol{n}} (\boldsymbol{n} \otimes \boldsymbol{n} - \frac{1}{3} I) \boldsymbol{e}_3 f_1 d\boldsymbol{n} \\
&\overset{(70)}{=} \frac{1}{24\pi} \int_{S^2} (\boldsymbol{n} \otimes \boldsymbol{n} - \frac{1}{3} I) \boldsymbol{e}_3 \Big[(\boldsymbol{n} \otimes \boldsymbol{n} - \frac{1}{3} I) \boldsymbol{e}_3 \cdot \nabla_{\boldsymbol{x}} \rho_0 + 3\rho_0 (\boldsymbol{n} \cdot \nabla_{\boldsymbol{x}} \boldsymbol{u}_0 \boldsymbol{n}) \Big] d\boldsymbol{n} \\
&= \frac{1}{24\pi} \int_{S^2} \begin{pmatrix} n_1 n_3 \\ n_2 n_3 \\ n_3^2 - \frac{1}{3} \end{pmatrix} \Big[(3\rho_0 w_{0x} + \rho_{0x}) n_1 n_3 + (3\rho_0 w_{0y} + \rho_{0y}) n_2 n_3 \Big] d\boldsymbol{n}
\end{aligned}$$

Observe that, due to symmetry considerations, the integrals

$$\begin{aligned}
\int_{S^2} n_1 n_3^3 - \frac{1}{3} n_1 n_3 d\boldsymbol{n} = 0 \\
\int_{S^2} n_2 n_3^3 - \frac{1}{3} n_2 n_3 d\boldsymbol{n} = 0 \\
\int_{S^2} n_1 n_2 n_3^2 d\boldsymbol{n} = 0,
\end{aligned}$$

while the remaining integrals are computed via spherical coordinates

$$\begin{aligned}
\int_{S^2} n_1^2 n_3^2 d\boldsymbol{n} = \int_0^\pi \sin^3\theta \cos^2\theta \, d\theta \int_0^{2\pi} \cos^2\varphi d\varphi = \frac{4\pi}{15} \\
\int_{S^2} n_2^2 n_3^2 d\boldsymbol{n} = \int_0^\pi \sin^3\theta \cos^2\theta \, d\theta \int_0^{2\pi} \sin^2\varphi d\varphi = \frac{4\pi}{15}.
\end{aligned}$$

We conclude that

$$I_1 = \frac{1}{90} \left(3\rho_0 w_{0x} + \rho_{0x} \, , \; 3\rho_0 w_{0y} + \rho_{0y} \, , 0 \right)^T$$

and that ρ_0 satisfies the equation

$$\begin{aligned}
\partial_t \rho_0 &= \frac{1}{30} \left(\partial_x \left(\frac{1}{3} \rho_{0x} + \rho_0 w_{0x} \right) + \partial_y \left(\frac{1}{3} \rho_{0y} + \rho_0 w_{0y} \right) \right) + \gamma \frac{4}{3} \Delta_{(x,y)} \rho_0 \\
&= \frac{1}{30} \nabla_{(x,y)} \cdot \left(\rho_0 \nabla_{(x,y)} w_0 \right) + \frac{1}{3} \left(4\gamma + \frac{1}{30} \right) \triangle_{(x,y)} \rho_0
\end{aligned}$$

Finally, we derive the evolution equation for w_0. From (64) we obtain

$$\partial_x p_0 = \partial_y p_0 = 0 \tag{71}$$

$$Re \partial_t w_0 - \Delta_{(x,y)} w_0 + \partial_z p_0 = -\rho_0. \tag{72}$$

Since the right hand side of (72) depends only on (x, y), the pressure is of the form $p = -\kappa(t) z$, where $\kappa(t)$ reflects the effect of an imposed pressure gradient. If there is no imposed pressure gradient and the boundary conditions ensure conservation of density (e.g. periodic) then the

pressure is hydrostatic and we may select $\kappa(t) := \bar{\rho} = \frac{1}{|D|}\int_D \rho(t,x,y)dxdy$ the conserved density. For periodic boundary conditions and for the case $\gamma = 0$, the functions (ρ_0, w_0) solve the coupled system

$$\begin{aligned} \partial_t \rho_0 &= \frac{1}{30}\nabla_{(x,y)} \cdot \left(\rho \nabla_{(x,y)} w_0\right) + \frac{1}{90}\Delta_{(x,y)}\rho_0 \\ Re\, \partial_t w_0 &= \Delta_{(x,y)} w_0 + (\bar{\rho} - \rho_0), \end{aligned} \tag{73}$$

where $\bar{\rho}$ is the average density.

B Appendix: Linear stability theory

In this appendix we study the linear stability of the shear flow problem and give an asymptotic expansion of the most unstable eigenvalue of the linear system in the Reynolds number Re.

We linearize the moment closure system (38)-(41) around the state $w = 0$ and $\rho = 1$ and consider the simplest case $\gamma = 0$, $D_r = 1$, which gives

$$\begin{aligned} \partial_t \rho &= \partial_x s \\ \partial_t c &= -4c \\ \partial_t s &= \frac{1}{8}\partial_x \rho + \frac{1}{4} w_x - 4s \\ Re \partial_t w &= \partial_{xx} w - \delta \rho. \end{aligned} \tag{74}$$

We take the Fourier transformation of (74) and consider first the case $Re = 0$. The last equation of (74) gives

$$\xi^2 \hat{w}(\xi) = -\delta \hat{\rho}(\xi), \tag{75}$$

while the remaining once lead to

$$\partial_t \begin{pmatrix} \hat{\rho} \\ \hat{c} \\ \hat{s} \end{pmatrix} = \begin{pmatrix} 0 & 0 & i\xi \\ 0 & -4 & 0 \\ \frac{1}{8} i\xi - \frac{i\delta}{4\xi} & 0 & -4 \end{pmatrix} \begin{pmatrix} \hat{\rho} \\ \hat{c} \\ \hat{s} \end{pmatrix}. \tag{76}$$

The matrix on the right of (76) has the eigenvalues

$$\left\{ -4, -2 - \frac{1}{4}\sqrt{64 + 4\delta - 2\xi^2}, -2 + \frac{1}{4}\sqrt{64 + 4\delta - 2\xi^2} \right\}.$$

The last eigenvalue, which we denote by λ_0, is larger than zero provided that $\delta > 0$ and ξ^2 is small enough. Thus, the linear moment closure system coupled with the Stokes equation is most unstable for waves with wave number $\xi \to 0$. The eigenvector corresponding to the eigenvalue λ_0 has the form

$$\boldsymbol{x}_0 = \left(\frac{2i\xi}{2\delta - \xi^2} \left(8 + \sqrt{64 + 4\delta - 2\xi^2} \right), 0, 1 \right)^T.$$

Now we consider the case $Re > 0$, for which the linearized coupled system can be expressed in the form

$$\begin{pmatrix} \dot{\boldsymbol{x}} \\ \dot{y} \end{pmatrix} = \begin{pmatrix} A & B \\ \frac{1}{Re} D & \frac{1}{Re} C \end{pmatrix} \begin{pmatrix} \boldsymbol{x} \\ y \end{pmatrix}. \tag{77}$$

with $\boldsymbol{x} = (\hat{\rho}, \hat{c}, \hat{s})^T$, $y = \hat{w}$ and

$$A = \begin{pmatrix} 0 & 0 & i\xi \\ 0 & -4 & 0 \\ \frac{1}{8}i\xi & 0 & -4 \end{pmatrix}, B = \begin{pmatrix} 0 \\ 0 \\ \frac{1}{4}i\xi \end{pmatrix}, D = \begin{pmatrix} -\delta & 0 & 0 \end{pmatrix}, C = -\xi^2.$$

Our goal is to give an asymptotic expansion for eigenvalues of the matrix arising on the right hand side of (77), which is valid for small values of Re. For $\varepsilon = \frac{1}{Re}$ we consider the ansatz

$$\begin{aligned} A\boldsymbol{x}_\varepsilon + By_\varepsilon &= \lambda_\varepsilon \boldsymbol{x}_\varepsilon \\ Cy_\varepsilon + D\boldsymbol{x}_\varepsilon &= \varepsilon\lambda_\varepsilon y_\varepsilon, \end{aligned} \tag{78}$$

set

$$\lambda_\varepsilon = \lambda_0 + \varepsilon\lambda_1 + \dots, \quad \boldsymbol{x}_\varepsilon = \boldsymbol{x}_0 + \varepsilon\boldsymbol{x}_1 + \dots, \quad y_\varepsilon = y_0 + \varepsilon y_1 + \dots.$$

and calculate the first two orders:

$$O(1): \qquad \begin{pmatrix} A - \lambda_0 I & B \\ D & C \end{pmatrix} \begin{pmatrix} \boldsymbol{x}_0 \\ y_0 \end{pmatrix} = \begin{pmatrix} 0 \\ 0 \end{pmatrix}, \tag{79}$$

$$O(\varepsilon): \qquad \begin{pmatrix} A - \lambda_0 I & B \\ D & C \end{pmatrix} \begin{pmatrix} \boldsymbol{x}_1 \\ y_1 \end{pmatrix} = \begin{pmatrix} \lambda_1 \boldsymbol{x}_0 \\ \lambda_0 y_0 \end{pmatrix}. \tag{80}$$

The left null space of the matrix on the left hand side of (80) is given by

$$\boldsymbol{u}^T = \left(-8 - \sqrt{64 + 4\delta - 2\xi^2}, 0, -4i\xi, 1\right). \tag{81}$$

We multiply both sides of Equation (80) from the left with $\boldsymbol{u}^T$ and obtain

$$0 = \boldsymbol{u}^T \cdot \begin{pmatrix} \lambda_1 \boldsymbol{x}_0 \\ \lambda_0 y_0 \end{pmatrix}. \tag{82}$$

From the second equation of (79) we obtain

$$y_0 = -C^{-1}D\boldsymbol{x}_0 = \frac{-2i\delta}{\xi} \frac{(8 + \sqrt{64 - 2\xi^2 + 4\delta})}{2\delta - \xi^2}.$$

Using the expressions for λ_0, $\boldsymbol{x}_0$, y_0 and $\boldsymbol{u}$ in Equation (82), we can now calculate λ_1, which has the form

$$\lambda_1 = -\frac{\delta}{\frac{2\xi^2}{(2\delta - \xi^2)}(8 + \sqrt{64 + 4\delta - 2\xi^2})^2 + 4\xi^2}. \tag{83}$$

In Figure 5(a) we plot the eigenvalue λ_0 as a function of the wave number ξ. This eigenvalue describes the linear stability behavior of the system for $Re = 0$. The longest possible waves are most unstable and there is no wave length selection. In Figure 5(b), we plot $\lambda_0 + Re\lambda_1$ vs. the wave number ξ for $\varepsilon = Re = 1$ and $\delta = 0.2$. A non-zero Reynolds number provides a wave length selection mechanism. The curve attains its maximum for a wave number $\xi \approx 0.27$. Thus, the linear theory predicts the wave length of the most unstable wave to be approximately $2\pi/0.27 \approx 23.27$. On an interval of length 100, we expect the formation of 4-5 clusters. This is in agreement with our numerical result shown in Section 6, Figure 4.

Acknowledgements Research supported in part by the King Abdullah University of Science and Technology (and by the Aristeia program of the Greek Secretariat for Research.

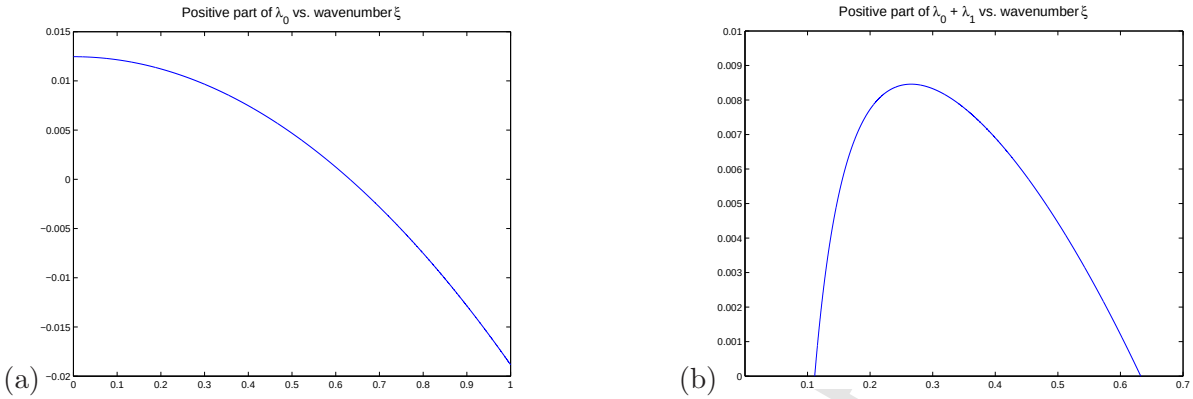

Figure 5: Positive part of the (a) λ_0 and (b) $\lambda_0 + \lambda_1$ vs. wave number ξ for $\delta = 0.2$.

References

[1] R.B. Bird, Ch.F. Curtiss, R.C. Armstrong, and O. Hassager. *Dynamics of Polymeric Liquids, Vol. 2, Kinetic Theory*. Wiley Interscience, 1987.

[2] J.-A. Carillo, Th. Goudon and P. Lafitte. Simulation of fluid and particles flows: Asymptotic preserving schemes for bubbling and flowing regimes. *J. Comput. Physics*, 227 (2008) 7929-7951.

[3] F.A.C.C. Chalub, P.A. Markowich, B. Perthame, and C. Schmeiser. Kinetic models for chemotaxis and their drift-diffusion limits. *Monatsh. Math.*, 142 (2004), 123–141.

[4] M. Doi and S.F. Edwards. *The Theory of Polymer Dynamics*. Oxford University Press, 1986.

[5] É. Guazzelli and J. Hinch. Fluctuations and instability in sedimentation. *Annu. Rev. Fluid Mech.*, 42 (2011), 97-116.

[6] Th. Goudon. Hydrodynamic limit for the Vlasov-Poisson-Fokker-Planck system: Analysis of the two-dimensional case. *Math. Mod. Meth. Appl. Sci.*, 15 (2005), 737-752.

[7] C. Helzel and F. Otto. Multiscale simulations for suspensions of rod-like molecules. *J. Comput. Phys.*, 216(1):52–75, 2006.

[8] Ch. Helzel and A.E. Tzavaras. A kinetic model for the sedimentation of rod-like particles. 2015 (submitted).

[9] B. Herzhaft and É. Guazzelli. Experimental study of the sedimentation of a dilute fiber suspension. *Physical Review Letters*, 77 (1996), 290-293.

[10] B. Herzhaft and É. Guazzelli. Experimental study of the sedimentation of dilute and semi-dilute suspensions of fibers. *J. Fluid Mech.*, 384 (1999), 133-158.

[11] D.L. Koch and E.S.G. Shaqfeh. The instability of a dispersion of sedimenting spheroids. *J. Fluid Mech.*, 209 (1989), 521-542.

[12] B. Metzger, J.E. Butlerz and É. Guazzelli. Experimental investigation of the instability of a sedimenting suspension of fibers. *J. Fluid Mech.*, 575 (2007), 307-332.

[13] H.G. Othmer and T. Hillen. The diffusion limit of transport equations II: Chemotaxis equations. *SIAM J. Appl. Math.* **62** (2002), 1222-1250.

[14] F. Otto and A. Tzavaras. Continuity of velocity gradients in suspensions of rod-like molecules. *Comm. Math. Phys.*, 277(3):729–758, 2008.

[15] F. Poupaud and J. Soler. Parabolic limit and stability of the Vlasov-Poisson-Fokker-Planck system. *Math. Mod. Meth. Appl. Sci.* **10** (2000), 10271045.

Highlights of the paper

A comparison of macroscopic models describing the collective response of sedimenting rod-like particles in shear flow

by Christiane Helzel and Athanasios E. Tzavaras

- Presentation of a kinetic multi-scale model, describing the sedimentation of rod-like particles
- Derivation of macroscopic models, which describe the collective behavior of the system
- A linear stability analysis, which predicts instability and a wavelength selection mechanism
- Numerical simulations, which compare the macroscopic models with the kinetic model